The Astronomical Journal, 147:1 (11pp), 2014 January doi:10.1088/0004-6256/147/1/1

ABSOLUTE PROPERTIES OF THE TRIPLE STAR HP AURIGAE

Claud H. Sandberg Lacy[1], Guillermo Torres[2], Marek Wolf[3], and Charles L. Burks[1]
[1] Physics Department, University of Arkansas, Fayetteville, AR 72701, USA; clacy@uark.edu, clburks@email.uark.edu
[2] Harvard-Smithsonian Center for Astrophysics, 60 Garden Street, Cambridge, MA 02138, USA; gtorres@cfa.harvard.edu
[3] Astronomical Institute, Faculty of Mathematics and Physics, Charles University in Prague,
180 00 Praha 8, V Holesovickach 2, Czech Republic; wolf@cesnet.cz
Received 2013 August 21; accepted 2013 October 14; published 2013 November 21

ABSTRACT

New photometric, spectroscopic, and eclipse timing observations of the eclipsing binary star HP Aur allow for very accurate orbital determinations, even in the presence of a third body and transient starspot activity. The eclipsing binary masses are determined to an accuracy of ±0.4% and the radii to ±0.6%. The masses are 0.9543 ± 0.0041 and 0.8094 ± 0.0036 solar masses, and the radii are 1.0278 ± 0.0042 and 0.7758 ± 0.0034 solar radii, respectively. The orbital period in the outer orbit is accurately determined for the first time: 4.332 ± 0.011 yr. A comparison with current theories of stellar evolution shows that the components' absolute properties can be well-matched by the current models at an age of about 7 billion years.

Key words: binaries: eclipsing – binaries: spectroscopic – stars: fundamental parameters – stars: individual (HP Aur)

Online-only material: machine-readable and VO tables

1. INTRODUCTION

Eclipsing binary stars have the potential to provide very accurate measurements of their components' masses, radii, luminosities, and temperatures, among other fundamental stellar parameters, which may be used to critically test stellar evolution theory. In order to determine these parameters with very high accuracy, accurate and plentiful measurements are needed of the brightness variations over time (the light curve) and radial velocity variations over time (the radial velocity curve). Complications can arise that make the analysis of these fundamental data more difficult: the stars may have transient spots that cause the system's brightness to change in an irregular fashion, or there may be a faint third body in the system that causes the times of minima to vary in a cyclic manner over time. Indeed, in HP Aur we have both of these types of complications, but have nevertheless been able to accurately determine mean absolute properties for the components.

The detached main-sequence eclipsing binary star HP Aur (HD 280603, TYC 2401–1263–1) is a relatively bright star (V = 11.187 mag), originally classified as G0. It was first discovered photographically as a variable star by Strohmeier (1958). The first B- and V-band photoelectric observations were made by Meinunger (1980), and several other light curves based on typically 200–300 photometric or CCD observations have been made since then. Meinunger measured the orbital period as 1.4228132 days. The first radial velocity measurements were those of Popper (2000). He summarized the state of the five existing photometric light curve studies at that time as "completely inadequate to evaluate the parameters of its light curve." Some of the photometric studies invoke orbital eccentricity (first asserted by Meinunger 1980), apsidal motion in an eccentric orbit (first asserted by Kozyreva 1990), a faint third component with a 13.7 yr period (Kozyreva et al. 2005), and spots/chromospheric activity (Liu et al. 1989; Eker et al. 2008).

Our current study is based on the analysis of 184 very accurate dates of minimum light and a large number (27) of new high-resolution spectrograms plus Popper's (2000) previously published ones (28), combined with a very large number (6685+2472) of new differential magnitudes obtained by two different and independent robotic telescopes. These new results are more definitive than in previous studies, and are accurate to better than 0.4% in the masses and 0.6% in the radii. The new and previously published dates of minimum light are discussed in Section 2, the spectroscopic observations and reductions are discussed in Section 3, the combined spectroscopic and eclipse timing analysis is discussed in Section 4, the photometric study in Section 5, and the absolute properties and comparison to theory in Section 6.

2. TIMES OF MINIMUM LIGHT

Published times of minimum light, as well as our own new dates, are listed in Table 1. Only photoelectric or CCD results are given, since the older photographic data do not improve the fits significantly and just add noise. Our new previously unpublished dates of minima come from three observatories in the Czech Republic: Ondrejov (Ondřejov Observatory, Czech Republic: 0.65 m reflecting telescope with an SBIG ST-8 or Apogee AP7p CCD camera and Johnson R filter), Ostrava (Observatory and Planetarium of Johann Palisa, Ostrava, Czech Republic: 0.20 m or 0.30 m telescopes with an SBIG ST-8XME CCD camera and Johnson R filter), and ValMez (Valašské Meziříčí Observatory, Czech Republic: 0.30 m Celestron Ultima telescope with an SBIG ST-7 CCD camera and Johnson *VRI* filters). Most of them were measured from images taken through the R filter. The weights originally assigned to the new dates were converted into mean uncertainties by calibrating the assigned weights of the new data with the published uncertainties of original observations of the other dates. These new dates and the other published ones are used in Section 4 in a combined solution of the dates of minima and radial velocities to estimate many orbital parameters and minimum masses.

3. SPECTROSCOPIC OBSERVATIONS AND REDUCTIONS

HP Aur was observed spectroscopically at the Harvard-Smithsonian Center for Astrophysics (CfA) with an echelle instrument ("Digital Speedometer"; Latham 1992) attached to the 1.5 m Tillinghast reflector at the Fred L. Whipple

Table 1
Dates of Minimum Light for HP Aur

Type of Eclipse[a]	HJD − 2,400,000	Precision (days)	Ref.
1	42756.3475	0.0020	1
2	42805.4375	0.0020	1
2	43498.3465	0.0020	1
1	43577.3113	0.0020	1
2	43848.3595	0.0020	1
1	43850.4903	0.0020	1
1	46008.9135	0.0020	2
2	46013.8954	0.0020	2
1	46018.8732	0.0020	2
1	46041.6383	0.0020	2
1	46045.9068	0.0020	2
1	46068.6719	0.0020	2
2	46070.8100	0.0020	2
1	46353.2355	0.0004	3
2	46355.3694	0.0003	3
1	50008.4580	0.0002	3
2	50010.5913	0.0001	3
2	50013.4379	0.0004	3
1	50099.5175	0.0001	3
2	51080.5584[b]	0.0001	4
2	51124.6623	0.0003	4
1	51196.5140	0.0001	4
1	51425.5903	0.0010	5
1	51876.6186	0.0003	6
2	51901.517	0.0010	6
2	51935.6673[b]	0.0001	7
1	51937.7984[b]	0.0001	8
1	51983.3303	0.0003	6
1	51987.5985	0.0002	8
2	52005.385	0.0005	6
2	52217.38704	0.0005	6
1	52219.52114	0.0002	6
2	52252.9581	0.0003	9
1	52263.6290	0.00007	9
1	52267.8979	0.00013	9
1	52270.7433	0.00014	9
1	52287.8168	0.0003	9
1	52300.6208	0.0008	8
2	52302.7587	0.0004	9
1	52317.6964	0.0002	9
1	52320.5422	0.0001	8
2	52332.6364	0.0002	9
1	52337.6167	0.0002	8
1	52374.6094	0.0001	8
1	52549.61648	0.0003	6
1	52563.8448	0.00016	9
1	52606.5288	0.0003	10
1	52607.9520	0.00018	9
2	52615.7779	0.0006	9
2	52618.6247	0.0005	8
1	52630.7169	0.0003	11
1	52683.36123	0.0003	6
2	52688.34145	0.0003	6
2	52695.459[b]	0.0001	12
1	52714.6626	0.0002	8
2	52729.60329	0.00023	11
2	52935.91092	0.00015	11
1	52949.42708	0.0002	6
2	52971.48018	0.0002	6
2	52985.7101	0.0010	13
1	53074.6351	0.00011	13
2	53079.6147	0.00016	13
1	53279.51856	0.0002	6
2	53288.7669	0.0006	14
2	53315.8018	0.00016	15
1	53317.93503	0.00013	15
1	53323.6262	0.0006	14
1	53354.9284	0.0001	15

Table 1
(Continued)

Type of Eclipse[a]	HJD − 2,400,000	Precision (days)	Ref.
1	53369.1572	0.0020	16
1	53387.6521	0.0016	17
2	53388.3641	0.0006	17
1	53410.4180	0.0023	17
1	53434.6051	0.00011	15
2	53452.3913	0.0005	6
1	53436.0284	0.0006	18
1	53455.9500	0.0020	19
2	53462.3529	0.0019	20
1	53609.6144	0.0002	21
2	53648.7383	0.0008	14
2	53674.3522	0.0013	22
1	53704.9447	0.00008	23
1	53704.9449	0.00010	15
2	53709.9231	0.0002	15
1	53710.6358	0.00012	15
1	53710.6359	0.0001	14
1	53713.48108	0.0003	6
1	53714.9041	0.00016	15
2	53735.5350	0.0003	24
2	53758.30032	0.0002	6
2	53762.5689	0.0002	14
1	53764.7023	0.0003	24
1	53771.8161	0.0002	24
2	53776.7970	0.0003	24
2	53779.6425	0.0002	24
1	53781.7770	0.0002	24
2	53786.7573	0.0002	24
1	53797.42992	0.0003	6
2	53802.40763	0.0005	6
1	53811.6569	0.0002	24
2	53995.9131	0.0003	24
2	54015.8334	0.0005	14
2	54018.6771	0.0005	25
2	54022.9466	0.0003	24
2	54032.9059	0.0002	24
2	54049.9798	0.0001	24
2	54059.9401	0.0001	24
2	54069.8998	0.0003	24
1	54077.7262	0.0003	24
2	54085.5516	0.0023	26
1	54091.9536	0.0002	24
1	54094.7994	0.0002	24
1	54097.634[b]	0.0020	14
2	54109.7384	0.0004	24
2	54115.429	0.0008	27
1	54117.5646	0.0004	14
1	54131.7931	0.0003	24
1	54134.6376	0.0002	24
1	54134.6378	0.0002	24
2	54136.7722	0.0002	24
2	54139.6184	0.0001	14
1	54161.6709	0.0001	14
1	54167.3622	0.0001	28
2	54172.3407	0.0005	29
2	54172.3419	0.0005	30
2	54172.3437	0.0005	31
1	54204.35626	0.00040	25
1	54204.35696	0.00040	25
1	54204.35726	0.00020	25
1	54380.7840	0.0002	32
1	54387.8986	0.0003	33
1	54397.8588	0.0002	33
1	54404.9720	0.0002	33
1	54404.9722	0.0002	33
2	54428.4489	0.0003	31
2	54432.7178	0.0002	33
1	54447.6580	0.0001	32

Table 1
(Continued)

Type of Eclipse[a]	HJD − 2,400,000	Precision (days)	Ref.
2	54469.7110	0.0004	33
2	54486.7847	0.0007	33
1	54487.4952	0.0001	31
2	54489.6304	0.0003	33
1	54500.30126	0.00010	34
1	54500.30136	0.00010	34
2	54506.7046	0.0002	32
1	54521.6429	0.0002	33
2	54522.3559[b]	0.0001	35
2	54532.31511	0.0003	6
2	54536.5843	0.0004	33
1	54737.9104	0.0001	33
2	54769.9220	0.0002	33
1	54777.7496	0.0002	33
2	54779.8821	0.0003	33
1	54787.7094	0.0001	33
2	54789.8428	0.0003	33
1	54834.6609	0.0001	36
1	54844.6199	0.0003	37
2	54849.6013	0.0002	33
1	54857.4262	0.0001	38
2	54866.6736	0.0003	33
1	54881.6145	0.0002	33
1	54888.7294	0.0002	39
1	54908.6470	0.0002	33
2	55139.8572	0.0003	40
1	55147.6829	0.0002	41
2	55155.5075	0.0006	35
1	55181.8290	0.0002	42
1	55184.6746	0.0001	41
2	55206.7296	0.0001	41
1	55220.24663	0.0003	43
1	55241.5885	0.0002	41
2	55246.5697	0.0003	41
1	55251.5488	0.0007	42
1	55258.6627	0.0002	42
2	55462.8389	0.0003	42
2	55526.8674	0.0001	44
2	55596.5852	0.0003	45
1	55651.36299	0.0003	6
1	55803.606	0.003	46
1	55843.4443	0.0003	6
2	55855.53767	0.0003	6
2	55946.5998	0.0005	47
1	55957.26894	0.0003	6
1	56220.48903	0.0003	6
1	56294.47561	0.0003	6
2	56356.36826	0.0003	6

Notes.
[a] Eclipses of type 1 are the deeper eclipses when the hotter, more massive component (star 1) is being eclipsed by the cooler, less massive component (star 2).
[b] These dates were omitted from the final orbital fit due to very bad residuals.
References. (1) Meinunger 1980; (2) Liu et al. 1989; (3) Wolf & Sarounova 1996; (4) Biro & Borkovits 2000; (5) Agerer & Hubscher 2001; (6) this paper; (7) Nelson 2002; (8) Baldwin 2003; (9) Lacy 2002; (10) Borkovits et al. 2003; (11) Lacy 2003; (12) Borkovits et al. 2004; (13) Lacy 2004; (14) Baldwin & Samolyk 2007; (15) Lacy 2006; (16) Nagai 2005; (17) Hubscher et al. 2005; (18) Kim et al. 2006; (19) Nagai 2006; (20) Diethelm 2005; (21) Zejda et al. 2006; (22) Diethelm 2006; (23) Nelson 2006; (24) Lacy 2007; (25) Brat et al. 2007; (26) Hubscher & Walter 2007; (27) Hubscher 2007; (28) Hubscher et al. 2009; (29) Bozkurt 2011; (30) Diethelm 2007); (31) Borkovits et al. 2008; (32) Samolyk 2008; (33) Lacy 2009; (34) Brat et al. 2008; (35) Lampens et al. 2010; (36) Samolyk 2009; (37) Diethelm 2009; (38) Hubscher et al. 2010; (39) Nelson 2010; (40) Diethelm 2010; (41) Samolyk (2010); (42) Lacy 2011; (43) L. Šmelcer 2010, private communication; (44) Diethelm 2011; (45) Samolyk 2011; (46) Paschke 2012; (47) Diethelm 2012.

Observatory (Mount Hopkins, AZ). A total of 27 exposures were gathered between 2002 September and 2007 January with a resolving power of $R \sim 35{,}000$. A single echelle order was recorded with an intensified photon-counting Reticon detector, giving a spectral range of 45 A centered at 5187 A, and including the lines of the Mg I *b* triplet. The signal-to-noise ratios of the exposures ranged from 16 to 30 per resolution element of 8.5 km s^{-1}. The wavelength solutions were based on exposures of a Th–Ar lamp before and after each science exposure.

Radial velocities were derived using the two-dimensional cross-correlation algorithm TODCOR (Zucker & Mazeh 1994). The two templates (one for the more massive star and another for the less massive star) were selected from a library of synthetic spectra based on model atmospheres by R. L. Kurucz (see Nordstrom et al. 1994; Latham et al. 2002). The best match to the components was determined by seeking the maximum of the cross-correlation coefficient averaged over all exposures (see Torres et al. 2002). The template parameters that affect the velocities the most are the effective temperature and rotational broadening, while surface gravity and metallicity have a smaller effect. We adopted log g values of 4.5 for both components, which are close to our final results reported later, and we assumed solar metallicity. The optimal template match was found for temperatures of 5900 K and 5530 K for the more massive and less massive star, with estimated uncertainties of 100 K and 150 K, respectively, and rotational velocities of 41 ± 3 km s^{-1} and 30 ± 5 km s^{-1}.

The zero point of our velocity system was monitored regularly by means of exposures of the dusk and dawn sky, and small run-to-run corrections were applied as described by Latham (1992). Additionally, we performed numerical simulations as we have done in previous studies with similar spectroscopic material, to test for systematic effects caused by residual line blending as well as lines shifting in and out of our narrow spectral window as a function of orbital phase (see, e.g., Torres et al. 1997). These effects were found to be as large as 2 km s^{-1} for the more massive star and 6 km s^{-1} for less massive star, and corrections to the velocities were applied based on the simulations. These corrections increase the masses by about 6% for the more massive star and 4% for the less massive star. The final velocities in the heliocentric frame and individual uncertainties including all corrections are listed in Table 2. The median uncertainties are 1.5 km s^{-1} for the more massive star and 4.0 km s^{-1} for the less massive star.

The light ratio between the two stars was determined from our spectra following Zucker & Mazeh (1994). We obtained $L_2/L_1 = 0.31 \pm 0.02$ at the mean wavelength of the observations (5187 A), which is close to the *V* band.

The next section describes the evidence for a third body in the system, originally proposed by Kozyreva et al. (2005). We searched for lines of this star in our spectra using an extension of TODCOR to three dimensions (Zucker et al. 1995), but found no convincing evidence for it. We place an upper limit on its brightness of about 5% of the light of the more massive star, assuming it is a sharp-lined main-sequence star, or it could possibly be a white dwarf and would be undetectable by us.

An additional set of radial velocities of HP Aur was obtained by Popper (2000) between 1988 and 1997. They include corrections for systematics analogous to those we applied, and are of similar quality as ours, with formal uncertainties of 2.6 km s^{-1} for the more massive star and 2.5 km s^{-1} for the less massive star. These measurements were incorporated into our orbital solution described below in Section 4.

Table 2
CfA Radial Velocities of HP Aur

HJD − 2,400,000	RV_1	RV_2	Err_1	Err_2	Phase[a]
52532.0148	92.60	−72.30	1.59	4.26	0.6307
52537.9393	119.17	−102.18	1.57	4.18	0.7946
52566.9004	−70.18	119.19	2.31	6.19	0.1493
52569.8456	−82.32	145.77	1.75	4.69	0.2193
52653.7980	−83.68	134.54	1.65	4.41	0.2235
52658.8325	124.92	−112.65	1.64	4.37	0.7619
52685.7124	105.02	−80.02	1.50	4.02	0.6539
52686.7634	−47.65	96.86	1.55	4.15	0.3926
52713.7054	−74.09	128.19	1.33	3.55	0.3282
52718.6213	121.45	−112.72	1.93	5.15	0.7833
52720.6095	−77.06	124.23	1.61	4.29	0.1806
52743.6260	−63.90	114.96	1.70	4.55	0.3573
52745.6289	121.85	−107.36	1.62	4.33	0.7650
52747.6270	−71.53	123.61	1.75	4.69	0.1693
52889.9806	−86.83	142.41	1.51	4.05	0.2197
52958.9859	118.23	−98.66	1.67	4.46	0.7186
52983.8684	−81.70	137.86	1.41	3.76	0.2068
52986.8520	−79.91	134.92	1.33	3.55	0.3038
52988.9342	119.00	−104.45	1.68	4.50	0.7672
53011.7770	113.36	−93.74	1.45	3.87	0.8218
53013.8372	−85.65	133.85	1.64	4.37	0.2698
53016.8065	−64.67	115.17	1.81	4.85	0.3567
53035.7268	104.98	−87.44	1.48	3.96	0.6544
53046.6221	−78.88	134.85	1.57	4.18	0.3120
54072.8470	64.93	−31.26	1.27	3.39	0.5733
54101.7442	91.23	−71.82	1.42	3.79	0.8831
54107.8219	−67.07	117.44	1.64	4.37	0.1547

Note. [a] Phase in the inner orbit as computed from the ephemeris in Table 3.

Table 3
Radial Velocity/Eclipse Timing Orbital Solution

INNER ORBIT	
Adjusted quantities	
P	$1.422819805 \pm 0.000000039$ days
γ	$+19.77 \pm 0.15$ km s^{-1}
K_1	104.87 ± 0.22 km s^{-1}
K_2	123.66 ± 0.24 km s^{-1}
Min I	$2{,}453{,}519.977385 \pm 0.000094$ (HJD)
Derived quantities	
$M_1 \sin^3 i$	$0.9520 \pm 0.0041\ M_{\rm Sun}$
$M_2 \sin^3 i$	$0.8074 \pm 0.0036\ M_{\rm Sun}$
q	0.8481 ± 0.0025
$a_1 \sin i$	$2.0518 \pm 0.0043\ 10^6$ km
$a_2 \sin i$	$2.4193 \pm 0.0047\ 10^6$ km
$a \sin i$	$4.4711 \pm 0.0062\ 10^6$ km
$a \sin i$	$6.4271 \pm 0.0088\ R_{\rm Sun}$
OUTER ORBIT	
Adjusted quantities	
P	1582.1 ± 4.0 days
K_3	3.46 ± 0.23 km s^{-1}
e	0.471 ± 0.050
ω	318.3 ± 4.8 deg
$T_{\rm peri}$	$2{,}450{,}403 \pm 20$ (HJD)
Derived quantities	
$M_3 \sin i$	$0.1669 \pm 0.0066\ (M_1{+}M_2{+}M_3)^{2/3}\ M_{\rm Sun}$
$a_{12} \sin i$	$66.3 \pm 2.6\ 10^6$ km
$a_{12} \sin i/c$	0.00256 ± 0.00010 days
Other quantities pertaining to the fit	
$\sigma_{\rm RV}$ (CfA)	1.5/4.0 km s^{-1}
$\sigma_{\rm RV}$ (Popper)	1.3/1.1 km s^{-1}
$N_{\rm RV}$ (CfA/Popper)	27/28
$N_{\rm ecl}$ (Min I/Min II)	101/75
Time span	37.2 yr

4. RADIAL VELOCITY/ECLIPSE TIMING ORBITAL SOLUTION

A diagram of the eclipse timing residuals from a linear ephemeris displays obvious periodic oscillations, particularly among the more recent timings that have better measurement errors. This strongly suggests a light travel time effect due to a third body in the HP Aur system. The radial velocities are likely affected at some level as well, which could potentially bias the mass determination. On the other hand, the velocities may contain useful information to help constrain the outer orbit, so we proceed here with a joint analysis of the eclipse timings and the velocities.

As a first step, we carried out spectroscopic orbital solutions separately for the CfA and Popper velocities to check for systematic differences. The agreement in the velocity amplitudes, which determine the masses, is excellent: the CfA observations give $K_1 = 104.61 \pm 0.35$ km s^{-1} and $K_2 = 124.08 \pm 0.93$ km s^{-1}, while those of Popper yield $K_1 = 104.42 \pm 0.59$ km s^{-1} and $K_2 = 124.14 \pm 0.56$ km s^{-1}. The resulting minimum masses differ by less than 0.3%. We did find an apparently significant difference in the center-of-mass velocities (which are $+18.18 \pm 0.29$ km s^{-1} for CfA and $+19.94 \pm 0.38$ km s^{-1} for Popper) that could be instrumental in nature, but this could also be due to orbital motion in the outer orbit.

We then combined both velocity data sets with the eclipse timings into a global solution, solving simultaneously for the elements of the inner and outer orbits (12 free parameters). We included one additional free parameter to represent a possible difference between the instrumental zero points of the two velocity data sets, for a total of thirteen unknowns. The formulation for the effect that the third body has on the timings follows the work of Irwin (1952, 1959), and the joint solution was carried out using standard non-linear least-squares techniques (e.g., Press et al. 1992). The dates of the velocity observations were corrected for light travel time during the iterations. Individual weights were applied to all observations based on the internal errors. The eclipse timings with no published uncertainties were assigned an error (separately for the primary eclipse and secondary eclipse measurements) such that the χ^2 per degree of freedom for those measurements was close to unity. The formal uncertainties of the other data sets were adjusted by a multiplicative scale factor to achieve a similar condition. This was done separately for the more massive star and less massive star velocities from CfA and Popper (2000), as well as for the primary and secondary eclipse timings with published errors. The adjustment factors for the errors of the eclipse timings were 3.1 for the primary eclipses and 2.7 for the secondary eclipses. Those for the uncertainties of the CfA velocities were close to unity. The original errors of the Popper velocities, on the other hand, were found to be *overestimated* by factors of 2.0 and 2.3 for the more massive star and less massive star velocities, respectively. This is explained by the fact that those errors were based on the rms residuals from Popper's orbital fits, which did not account for perturbations caused by the third star, not known at the time. This resulted in an increased scatter (see below), noted also by Popper.

The elements we obtained for the inner and outer orbits are presented in Table 3. The outer orbit is fairly eccentric and has

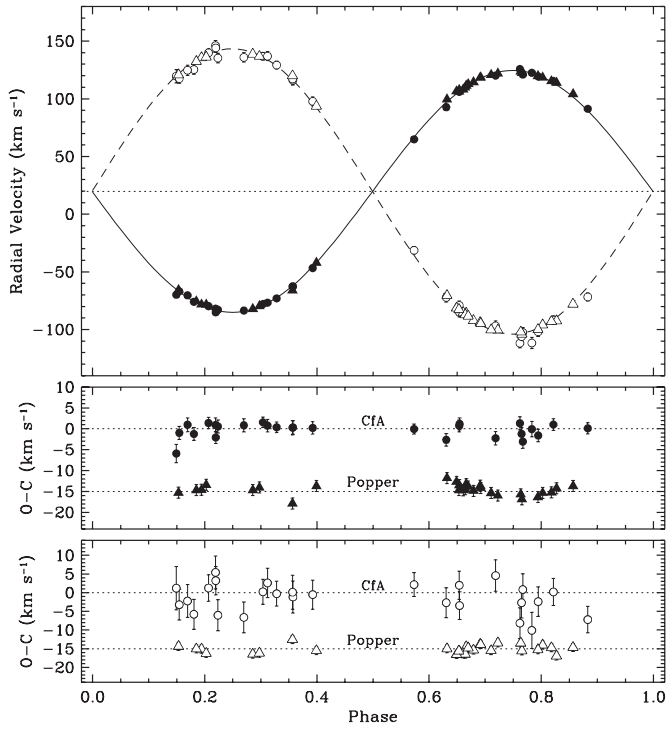

Figure 1. Radial velocity measurements for HP Aur from CfA and from Popper (2000), shown with circles and triangles, respectively, along with our best-fit model. Filled symbols and the solid line correspond to the more massive star 1. The dotted line represents the center-of-mass velocity of the triple system. Motion in the outer orbit has been subtracted from the measurements and from the model in the top panel. Residuals are shown in the bottom panels, with those from Popper displaced vertically for clarity. The more massive star 1 residuals from Popper (2000) show signs of a systematic trend, which is, however, not present in those of the less massive star 2.

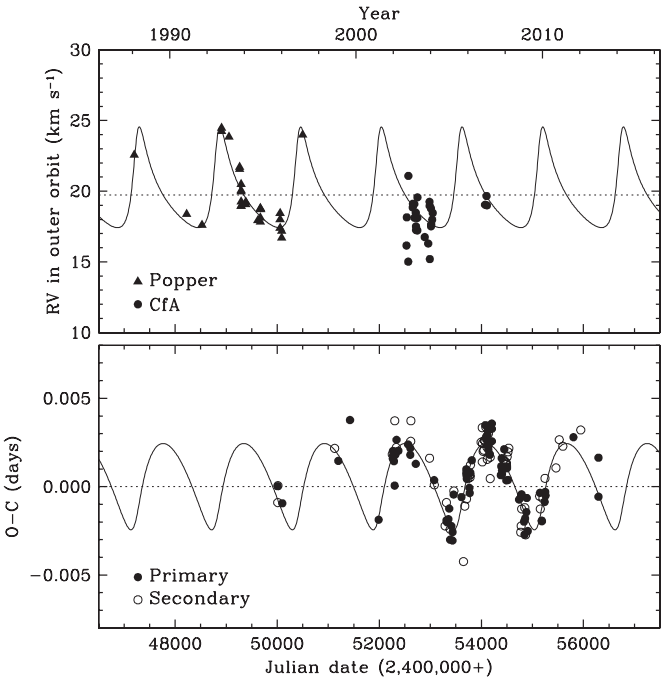

Figure 2. Motion of the center of mass of the eclipsing pair in the HP Aur system as traced by the radial velocity and eclipse timing observations obtained in the last 15 yr, along with our model for the outer orbit. A few older eclipse timings are not shown to avoid compressing the timescale. Top: the symbols correspond to the mean radial velocity of the inner binary's center of mass, computed as a weighted average of the primary and secondary velocities after subtracting the motion in the 1.4 day orbit. The larger dispersion for CfA is driven by the larger residuals of the secondary velocities in that data set compared to the Popper observations (see Table 3), when taking the average. The dotted line represents the center-of-mass velocity of the triple. Bottom: the bottom panel shows the light travel time curve with the $O - C$ residuals from the linear ephemeris given in Table 2. The semi-amplitude of this effect corresponds to about 3.7 minutes.

a period of about 4.3 yr, which is *very different* from the value of 13.7 yr proposed by Kozyreva et al. (2005). For our final fit, we considered the inner orbit to be circular. Test solutions in which we allowed the eccentricity to vary gave a value not significantly different from zero. Similarly, the offset between the zero points of the two velocity data sets was negligible when allowed to vary, so in the final fit we set it to zero. Figures 1 and 2 display the results.

As may be seen in Figure 2, the CfA velocities were all obtained over a relatively narrow range of phases in the outer orbit. Therefore, they are not much affected by the motion in the outer orbit, but also do not constrain it very much. The observations by Popper (2000), on the other hand, span two full cycles of the outer orbit and sample most phases well. This explains why they are more affected by the changing center of mass of the eclipsing pair, which led Popper to overestimate his errors, which were based on the dispersion from a double-lined orbital fit. Conversely, these velocities provide strong constraints on the outer orbit that complement the timing measurements very well, as they cover an interval of time in which few eclipses were observed.

5. PHOTOMETRIC STUDY

Differential photometry was produced from images taken by two independent robotic telescopes. The URSA WebScope is built from a Meade 10 inch $f/6.3$ LX-200 telescope with a Santa Barbara Instruments Group ST8 CCD camera (binned 2 × 2 to produce 765 × 510 pixel images with 2.3 arcsec^2 pixels) inside a Technical Innovations Robo-Dome, and controlled with an Apple Macintosh G4 computer executing a nightly observing schedule. The observatory is located atop Kimpel Hall on the Fayetteville, Arkansas campus, with the control room located beneath the observatory inside the building. Exposures of 120 s through a Bessel V filter (2.0 mm of GG 495 and 3.0 mm of BG 39) were read out and downloaded to the control computer over a 30 s interval, then the next exposure was begun. The observing cadence was about 150 s per observation. The variable star would often be monitored continuously for 1–6 hr. HP Aur was observed by URSA on 132 nights during parts of 10 observing seasons from 2001 November 22 to 2010 September 23, yielding 6685 observations.

The other telescope we used is the NFO WebScope, a refurbished 24 inch Group 128 Cassegrain reflector with a 2K × 2K Kodak CCD camera, located near Silver City, NM (Grauer et al. 2008). Observations consisted of 120 s exposures through a Bessel V filter. HP Aur was observed by NFO on 68 nights during parts of four observing seasons from 2005 January 29 to 2008 February 27, yielding 2472 observations.

The images were flat-fielded and measured by an automated application (Measure, written by author Lacy). Extinction coefficients were determined nightly from the comparison star measurements. They averaged 0.26 mag/airmass at URSA (they ranged from 0.19 to 0.31 mag/airmass) and 0.19 mag/airmass at the NFO (they ranged from 0.13 to 0.26 mag/airmass). The comparison stars were TYC 2401–0760–1 (BD +69° 1005, $V_T = 10.695$ mag) and TYC 2401–0224–1 (HD 280491, $V_T = 10.343$ mag; K2). Both comparison stars are west of the variable star, but within 8 arcmin of it. The mean nightly

Table 4
URSA Differential Photometry of HP Aur

Orbital Phase	ΔV	HJD − 2,400,000
0.49966	1.003	52235.88202
0.50030	1.009	52235.88294
0.50093	1.021	52235.88384
0.50157	1.017	52235.88475
0.50222	1.020	52235.88567

(This table is available in its entirety in machine-readable and Virtual Observatory (VO) forms in the online journal. A portion is shown here for guidance regarding its form and content.)

Table 5
NFO Differential Photometry of HP Aur

Orbital Phase	ΔV[a]	HJD − 2,400,000
0.55061	1.633	53399.82141
0.55286	1.634	53399.82461
0.55517	1.633	53399.82790
0.55741	1.632	53399.83109
0.55970	1.636	53399.83434

Note. [a] The NFO differential magnitudes (variable-comparisons) are referenced to the magnitude corresponding to the sum of the flux of two comparison stars.

(This table is available in its entirety in machine-readable and Virtual Observatory (VO) forms in the online journal. A portion is shown here for guidance regarding its form and content.)

magnitude difference between the comparison stars was constant within a standard deviation of 0.028 mag (URSA) and 0.013 mag (NFO). The scatter in comparison star magnitude differences within a night averaged 0.007 mag (URSA) and 0.005 mag (NFO) for the standard deviation of the nightly differential magnitudes. For the differential magnitudes, URSA data uses the variable minus the first comparison star only, whereas for NFO data, the sum of the fluxes of both comparison stars was converted to a magnitude called "comparisons." The resulting 6685 (URSA) and 2472 (NFO) *V*-magnitude differences (variable-comparison or variable-comparisons) are listed in Tables 4 and 5 (without any nightly magnitude corrections or light travel-time corrections) and are shown in Figures 4–6 (after the nightly magnitude corrections and light travel-time corrections discussed below have been added). In terms of time coverage, the NFO observations lie in the middle half of the URSA observational coverage.

5.1. Photometric Orbit

Preliminary examination of the light curves showed relatively large (several hundredths of a mag) night-to-night and longer-period variations in the URSA and NFO data, ranging from nights to years; this had never occurred before with URSA light curves of many other eclipsing binary stars, so it is clearly intrinsic to the variable star itself. The light curve fitting was done with the Nelson–Davis–Etzel (NDE) model as implemented in the code *jktebop* (Etzel 1981; Popper & Etzel 1981; Southworth et al. 2007). An initial fit was made in order to get a preliminary mean light curve, from which it was possible to determine the mean residuals for each night. These mean residuals (observed − computed) are plotted in Figure 3. The binary appears to have become about 0.1 mag fainter over the last decade. The observed variations due to transient starspots are so rapid, random, and numerous that we cannot hope to model them accurately with our data set, but by subtracting off the mean of the nightly residuals from the preliminary light curve, we can get a mean light curve that will yield reliable mean parameters for further analysis.

The light curves that have the nightly residuals removed and also the light travel-time lags around the three-body center of mass removed are shown in Figures 4–6.

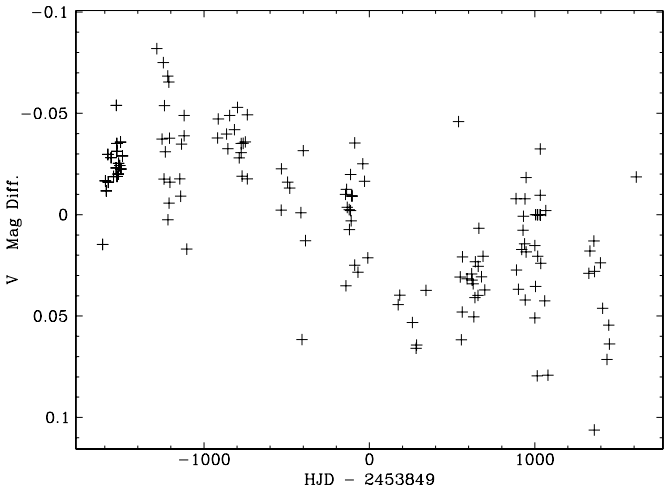

Figure 3. Variations in the light level of HP Aur over a 9 yr interval. Variations are seen over periods of days to years. The star has dimmed by roughly 0.1 mag over about a decade.

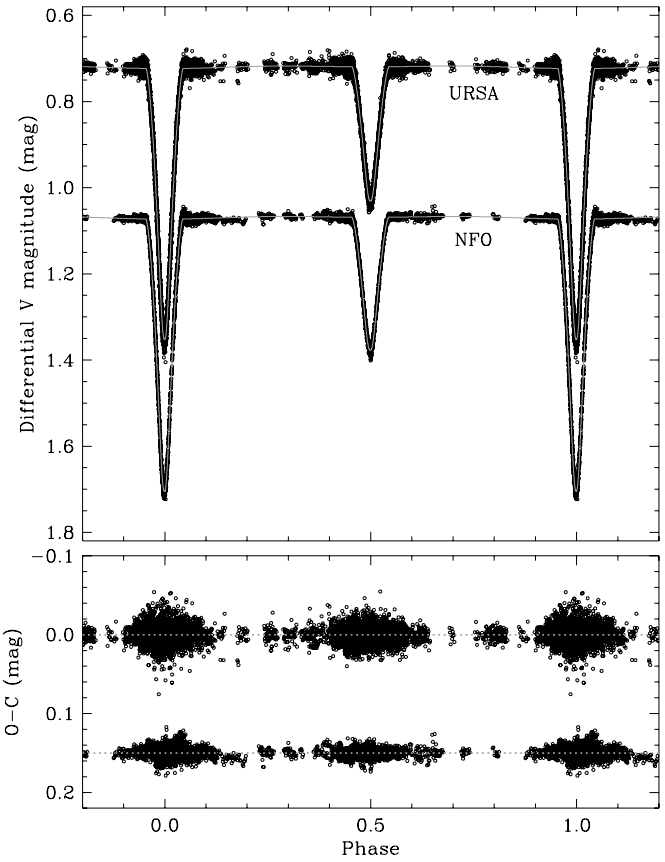

Figure 4. URSA and NFO mean light curves after removal of mean nightly residuals and time lags due to three-body motion around the center of mass.

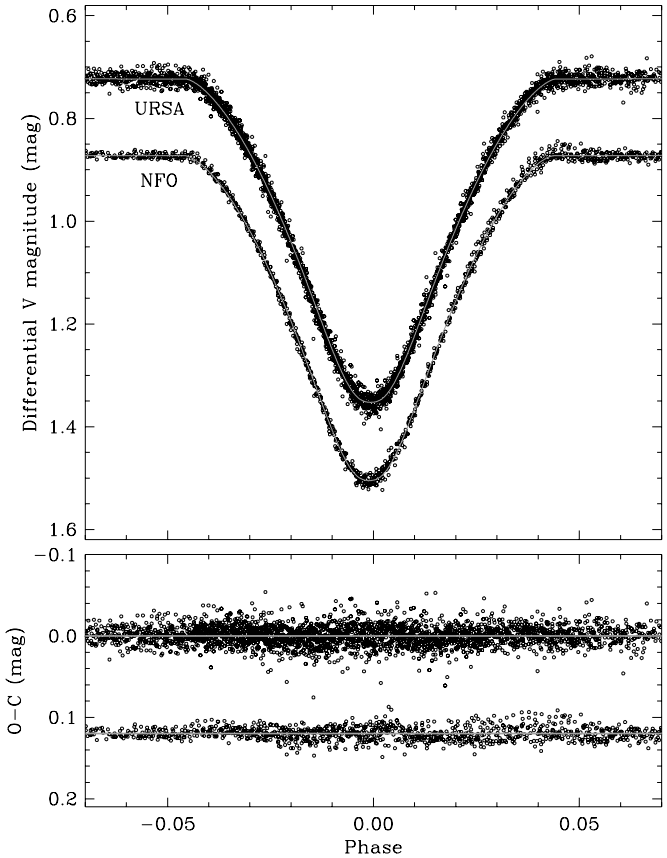

Figure 5. Primary (deeper) eclipse of HP Aur.

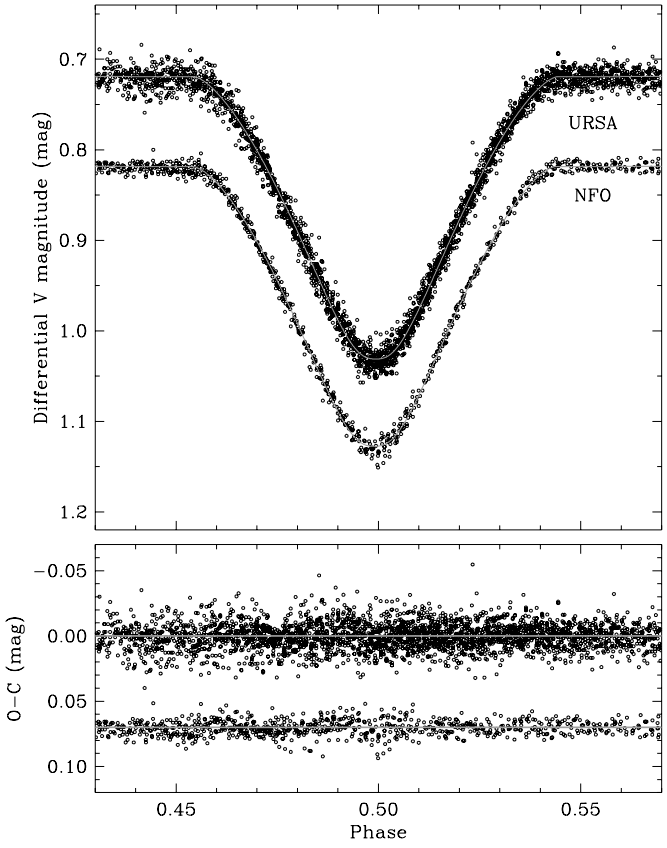

Figure 6. Secondary (shallower) eclipse of HP Aur.

Table 6
Photometric Orbital Elements for HP Aur

Element	URSA	NFO	Adopted
$J_2(V)$	0.5479 ± 0.0098	0.5501 ± 0.0112	0.549 ± 0.010
$r_1 + r_2$	0.2809 ± 0.0005	0.2800 ± 0.0005	0.2804 ± 0.0009
r_1	0.1599 ± 0.0003	0.1597 ± 0.0003	0.1598 ± 0.0007
r_2	0.1210 ± 0.0003	0.1203 ± 0.0003	0.1207 ± 0.0005
k	0.7566 ± 0.0016	0.7530 ± 0.0018	0.7548 ± 0.0036
i (deg)	87.716 ± 0.037	87.679 ± 0.042	87.698 ± 0.040
e	0 fixed	0 fixed	0
u_1	0.111 ± 0.025	0.193 ± 0.027	0.15 ± 0.04
u_2	0.043 ± 0.052	0.142 ± 0.059	0.09 ± 0.05
y_1	0.038 fixed	0.038 fixed	0.038
y_2	0.039 fixed	0.039 fixed	0.039
q	0.8481 fixed	0.8481 fixed	0.8481
L_3	0 fixed	0 fixed	0
L_1	0.7575 ± 0.0029	0.7595 ± 0.0028	0.7585 ± 0.0021
L_2	0.2425 ± 0.0029	0.2405 ± 0.0028	0.2415 ± 0.0021
L_2/L_1 (V)	0.3201 ± 0.0011	0.3166 ± 0.0014	0.318 ± 0.004
σ (mmag)	11.26821	6.91833	
N	6685	2472	
Corrections	132	73	

Photometric orbital elements resulting from the fits are given in Table 6. The principal fitted elements are $J_2(V)$, the visual central surface brightness of the cooler, smaller, less massive star 2; r_1+r_2, the sum of relative radii of the stars; k, the ratio of the smaller to larger radius; i, the orbital inclination in degrees; and u_1 and u_2, the limb-darkening coefficients. Auxiliary quantities related to the fit include L_1 and L_2, the normalized luminosities of the stars; σ, the standard error of an observation; N, the number of observations; and the number of corrections applied to the instrumental data. The value of the mass ratio was fixed at the spectroscopically fitted value. In finding the photometric solutions, we initially assumed that the limb-darkening coefficients would be near values predicted by atmospheric theory for stars of approximately the temperatures of ours, about 0.67 and 0.74 for the coefficients, and we fixed their values in the solutions. These solutions, however, had light ratios, L_2/L_1, near 0.6, which was far from the spectroscopic value, 0.31 ± 0.02 at V. Eventually it was decided that, because these stars were known from our observations of the variations in brightness over time to have spots and were reported as chromospherically active, the limb-darkening coefficients were likely to be non-standard, so we let them be variables in the solutions. The solutions then converged to values with light ratios near 0.318 ± 0.004 for limb-darkening values near 0.15 and 0.09. These unusually small limb-darkening values underscore the fact that this system has transient spots and chromospheric activity. The two independent sets (URSA and NFO) of fitted photometric orbital parameters do agree with each other remarkably well considering that they were derived from different telescopes at different times, and considering there are spot variations on a number of timescales in the raw data.

We have experimented with fitting orbits to other, much smaller, photometric data sets for HP Aur, those of Meinunger (1980; B and V), Kozyreva (1990; V), and M. Wolf (private communication; R). The general result is that the smaller data sets will not converge with the limb-darkening coefficients left as free variables because there are not enough high-quality data in the sets. By fixing the limb-darkening parameters to values near those derived from the URSA and NFO sets and then creating grids of solutions by varying the value of the ratio of the

radii, k, we can find solutions that have luminosity ratios L_2/L_1 in the range allowed by the independently measured spectroscopic light ratio. There are a few parameter differences that may possibly be significant, but the general results of the light curve analyses are similar between the various smaller data sets and the URSA and NFO data sets. Because the URSA and NFO sets are so much larger, their parameter uncertainties are very much smaller than the other sets, and we have chosen to use only these best data sets in our final analyses.

Lacy (1987) showed that the difference in visual surface brightness parameter, ΔF_v, is connected to the normalized V-band central surface brightness of the cooler star in eclipsing binaries ($J_1 = 1$): $\Delta F_v = 0.25 \log J_2'$. Here, J_2 is a fitted parameter in the *jktebop* code that models the light curves, and J_2' is that value corrected for differences in limb-darkening parameters. Popper's (1980) Table 1 gives the relationship between the visual surface brightness parameter F_v and the stellar temperature T, thus the difference in temperature ΔT is readily and very accurately determined from the V-filter light curve fit alone. Additional light curves in different bandpasses are not necessary to determine accurately the temperature difference determined by this surface-brightness method.

Tests for third light in both data sets showed that it is not detectable at a significant level. The radial velocity and eclipse timing data showed that the eccentricity in the short-period orbit is zero within the uncertainties, so that parameter was also fixed at zero in the final analyses.

The NDE model used by *jktebop* has been compared with more complicated models (Popper & Etzel 1981; North & Zahn 2004) including the WD model. The principal results of these studies are that the limits for high-accuracy measurements of parameters such as the radii, inclination, etc. with the NDE model are that the component oblateness should be less than 0.04 and the mean radii should be less than 0.25. Since the HP Aur properties are all well within these limits, we do not feel the need to use a more complicated model in this case.

6. ABSOLUTE PROPERTIES OF HP Aur

Our measured value of J_2 from the light curves enables a more precise determination of the temperature difference than that allowed by the spectroscopy (see the discussion about ΔF_v above). We obtain 660 ± 30 K using the visual flux calibration by Popper (1980). Our spectroscopic temperature for the more massive star of 5900 K then implies 5240 K for the less massive star. We note, however, that our spectroscopic estimates depend rather strongly on the adopted metallicity, for which we used the solar value in Section 3, as no other spectroscopic determination is available. An additional measure of the temperature that is much less sensitive to metallicity may be obtained from standard photometry available in the literature for the combined light, along with color–temperature calibrations from Casagrande et al. (2010). We used the following sources for the photometry: B_T and V_T from the *Tycho-2* Catalog (Hog et al. 2000), B and V from the APASS catalog (Henden et al. 2012), JHK_s from the 2MASS catalog (Cutri et al. 2003), V and I_C from the TASS catalog (Droege et al. 2006), B and V from Kozyreva et al. (2005), and a $B - V$ index from Liu et al. (1989). We constructed 10 different but non-independent color indices, and de-reddened them following Cardelli et al. (1989). An estimate of the reddening was obtained by consulting the dust maps by Schlegel et al. (1998), Drimmel et al. (2003), and Amores & Lepine (2005), from which we derived $E(B - V)$ values of 0.042, 0.039, and 0.064 mag, respectively, for an assumed distance of 210 pc (see below). The average reddening adopted is $E(B - V) = 0.048 \pm 0.020$, with a conservative uncertainty. We obtained a mean temperature for HP Aur of 5560 ± 100 K. Assuming this corresponds to the luminosity-weighted average of the two components, the flux scale of Popper (1980) results in a temperature of 5730 K for the more massive star and a value of 5100 K for the less massive star. Finally, we averaged our two estimates for the more massive star to obtain 5810 ± 120 K, and derived the temperature of the less massive star as 5160 ± 120 K from a slightly adjusted temperature difference based on J_2 (650 ± 30 K). The corresponding spectral types are approximately G2 and K1. The final temperature uncertainties for the more massive and less massive stars include a contribution of 100 K added in quadrature to account for possible systematics in our spectroscopic and photometric estimates. The absolute properties of HP Aur are given in Table 7.

Table 7
Absolute Properties of the Close Binary Stars in HP Aur

Parameter	Star 1	Star 2
Mass (solar masses)	0.9543 ± 0.0041	0.8094 ± 0.0036
Radius (solar radii)	1.0278 ± 0.0042	0.7758 ± 0.0034
log g (cm s^{-2})	4.3942 ± 0.0040	4.5669 ± 0.0043
Eccentricity e	0[a]	
v sin i (km s^{-1}) (observed value)	41 ± 3	30 ± 5
Circular v_{sync} (km s^{-1}) (equatorial)	36.5 ± 0.1	27.6 ± 0.1
Orbital semi-major axis a (solar radii)	6.432 ± 0.009	
T_{eff} (K)	5810 ± 120	5160 ± 120
log L (solar units)	0.036 ± 0.035	-0.414 ± 0.039
M_V (mag)	4.68 ± 0.12	5.94 ± 0.10
F_V	3.752 ± 0.012	3.687 ± 0.010
E_{B-V} reddening (mag)	0.048 ± 0.020	
$m - M$ (mag)	6.61 ± 0.15	
Distance (pc):		
from Popper (1980)	214 ± 13	
from Flower (1996)	209 ± 14	

Note. [a] The eccentricity e, when allowed to be a variable, was found to be 0.0006 ± 0.0016, so it was fixed at 0 in the final orbital fit.

A distance to HP Aur of 210 ± 15 pc was obtained by using the visual surface brightness parameter calibration of Popper (1980) and the average out-of-eclipse brightness ($V = 11.187 \pm 0.018$) corrected for extinction. This distance estimate is in good agreement with an independent one involving bolometric corrections from Flower (1996; see also Torres 2010).

The measured projected rotational velocities appear to be roughly consistent with the predicted synchronous values listed in Table 7. The M_3 sin i value in Table 3 along with the absolute masses of the more massive and less massive eclipsing stars lead to an estimated minimum mass for the tertiary of about 0.27 M_{Sun}, corresponding to a late-M dwarf (SpT approximately M4). On the other hand, from our spectroscopic limit on the brightness of this star in Section 3, its spectral type is not likely to be earlier than about M0 if it is a main-sequence star, implying an upper limit on the mass of around 0.5 M_{Sun} (unless it is a white dwarf).

7. COMPARISONS WITH THEORY

The accurate masses and radii of the eclipsing binary in HP Aur (see Table 7), along with the temperatures, permit a meaningful comparison with stellar evolution theory. To be conservative, the error estimates on the radii in Table 6 have

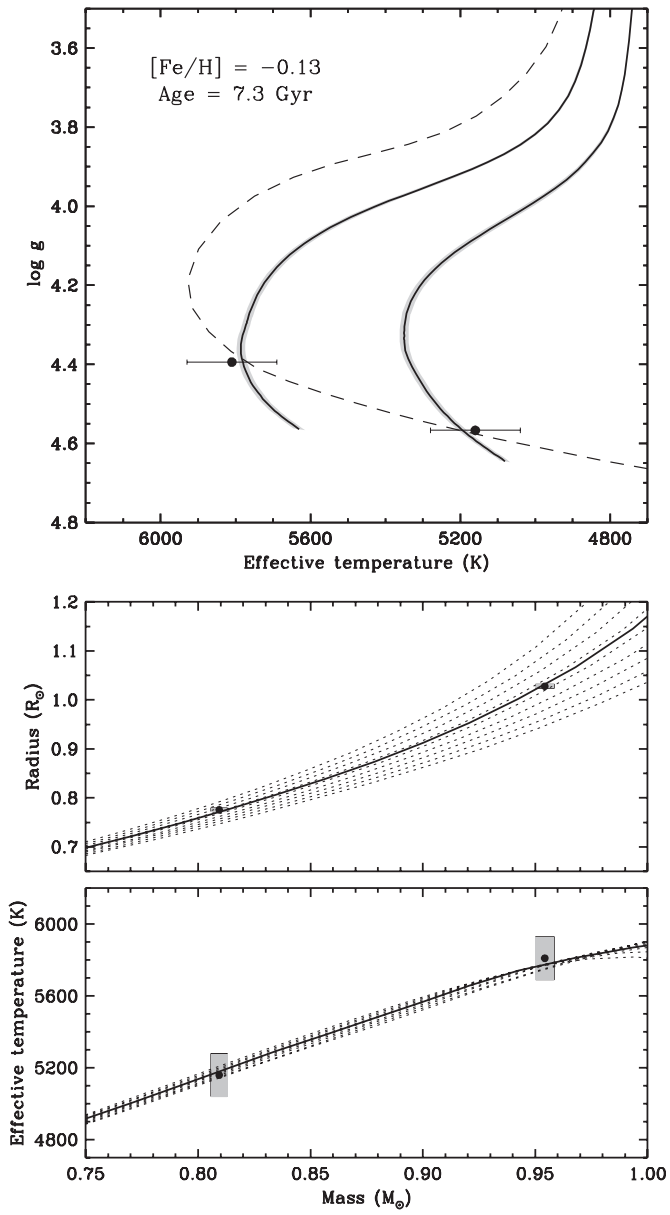

Figure 7. Observations of HP Aur compared against Yonsei-Yale models (Yi et al. 2001). Top: the solid lines show evolutionary tracks for the measured masses, with the gray areas around each track representing the uncertainty in their location that comes from the mass errors. The best-fit isochrone for a metallicity of [Fe/H] = −0.13 ($Z = 0.0136$) and an age of 7.3 Gyr is shown with a dashed line. Middle and bottom: radius and temperature as a function of mass. Isochrones for the same metallicity as above and ages between 5 and 9 Gyr are shown with dotted lines (in 0.5 Gyr steps), and the best-fit 7.3 Gyr isochrone is indicated with a thick solid line.

been doubled since the stars are variable over time. Figure 7 shows the observations against models from the Yonsei-Yale series (Yi et al. 2001).

The top panel displays evolutionary tracks for the measured masses, where we have adjusted the metal abundance of the models to match our estimated effective temperatures. The best-fit metallicity is $Z = 0.0136$, which in these models corresponds to [Fe/H] = −0.13 (assuming [α/Fe] = 0.0). All properties of both components are well fit at an age of 7.3 Gyr. The corresponding isochrone is shown with a dashed line. The lower panels of Figure 7 illustrate the agreement in radius and in temperature, with the solid line representing the same isochrone as in the top panel. The more massive star of the eclipsing binary has evolved considerably, and in terms of its age it is about 3/4 of the way to exhausting its central hydrogen. According to these models, the central helium abundance is $Y_c = 0.78$ (from a starting fraction of about $Y_c = 0.257$ at this metallicity). The lower-mass star, on the other hand, is only about 1/3 of the way to the terminal-age main sequence, and currently has a central helium fraction of $Y_c = 0.54$.

The Yonsei-Yale models adopt gray model atmospheres as boundary conditions between the photosphere and the interior. For stars of solar type or hotter this is a good approximation, but for cooler stars it has been shown that non-gray model atmospheres are needed for a more realistic representation of stellar structure (see, e.g., Chabrier & Baraffe 2000 and references therein). The less massive K1 star in HP Aur is cool enough that this may affect the comparison described above. We have therefore made an additional comparison using models from the Dartmouth series (Dotter et al. 2008), which use non-gray boundary conditions as well as a more sophisticated equation of state. Figure 8 shows that the Dartmouth models also provide an excellent fit to the observations, for a metallicity of [Fe/H] = −0.06 and an age of 7.0 Gyr, which are similar to those found earlier. All measured quantities agree with predictions to well within their uncertainties, including the well measured temperature difference.

The less massive star of HP Aur is near the regime where other low-mass stars in short-period binaries have shown discrepancies with stellar evolution models, in the sense of being larger and cooler than predicted. Objects displaying these disagreements have generally been found to be rapid rotators and to have high levels of chromospheric activity. HP Aur was detected as a strong X-ray source by *ROSAT* (Voges et al. 1999). Based on the measured count rate and hardness ratio HR1, we estimate its total X-ray luminosity to be $\log(L_X) = 30.4$, and the X-ray to bolometric luminosity ratio to be $\log(L_X/L_{bol}) = -3.35$. This value is near the observed saturation level for coronal X-ray sources of $\log(L_X/L_{bol}) \sim -3$ (see, e.g., Pizzolato et al. 2003), indicating the system is indeed very active, as might be expected from its short orbital period. Assuming the stars in HP Aur are rotationally synchronized, as appears to be the case, the Rossby numbers of the components (defined as the ratio between the rotation period and the convective turnover time) inferred from their spectral types ($\log R_0 = -1.2$ and -1.4 for the more massive and less massive stars) place both components in the range where stars usually present photometric variability due to spots (see Hall 1994). This is consistent with what we see in the light curves of HP Aur. Furthermore, both stars show the Ca II H and K lines in emission, and Hα is in absorption but filled in (Strassmeier et al. 1993).

Our model comparisons above give no indication of any significant discrepancies in radius or in temperature for the lower-mass star of the kind exhibited by other active stars, which is somewhat unexpected. Also unusual is the fact that the system appears quite old (∼7 Gyr), despite being very active. The indications that the more massive star is also an active star suggest the possibility that *both* components may be inflated and may have their temperatures suppressed by the high activity levels, but with anomalies that are similar in magnitude so that the stars still fall on a single isochrone. The larger mass of the more massive star (only 5% smaller than the Sun's) does not necessarily exempt it from possibly having these effects, which have been reported in a number of similarly active and well measured stars of about the same mass (e.g., V1061 Cyg B, FL Lyr B, CV Boo B, ZZ UMa B, and EF Aqr B, all with

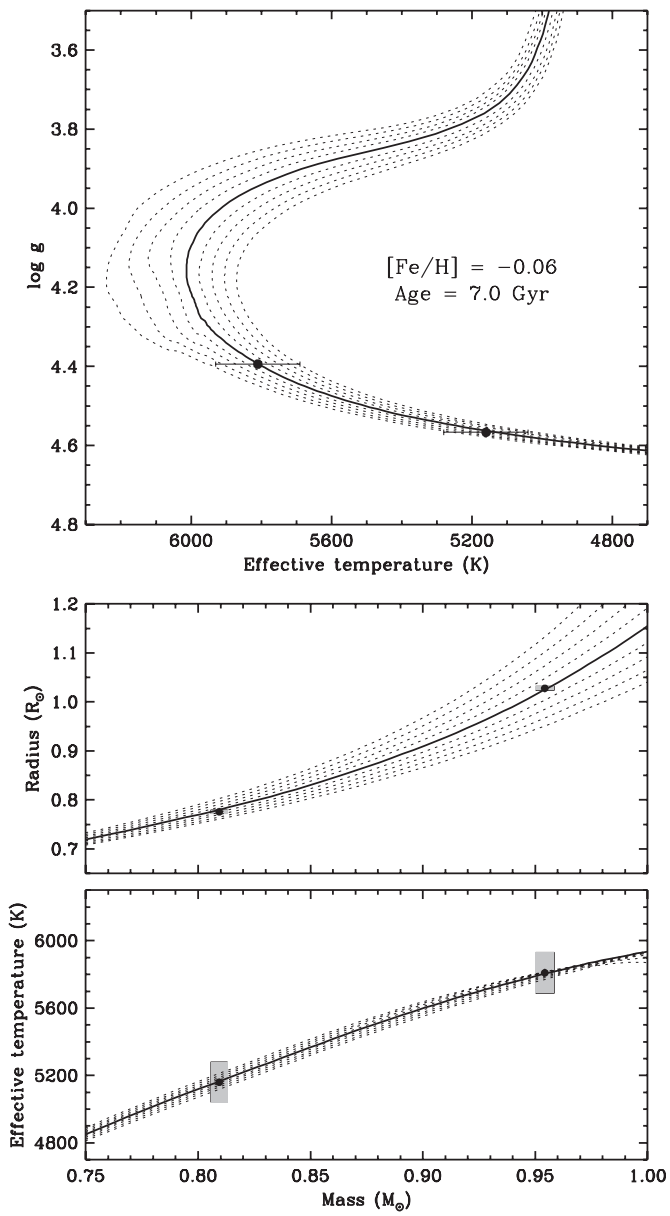

Figure 8. Similar to Figure 7 for the Dartmouth models of Dotter et al. (2008). Top: isochrones in 0.5 Gyr steps from 5 to 9 Gyr (left to right) are shown with dotted lines. The best-fit 7.0 Gyr model is represented with a solid line. Middle and bottom: same isochrones as above in the radius vs. mass and temperature vs. mass diagrams.

$M > 0.93 M_{\rm Sun}$; Torres et al. 2006, 2008; Clausen et al. 2009; Vos et al. 2012). We are unable to explore this hypothesis further with the evidence in hand because our model comparisons have two free parameters (age and metallicity), the combination of which can give a wide range of slopes for the mass–radius and mass–temperature relations. The issue could be resolved, however, with an accurate spectroscopic determination of the metallicity of HP Aur to remove the degeneracy.

The authors wish to thank Bill Neely, who operates and maintains the NFO WebScope for the Consortium, and who handles preliminary processing of the images and their distribution. We thank P. Berlind, M. Calkins, G. Esquerdo, and D. W. Latham for help in obtaining the CfA spectra, and R. J. Davis for maintaining the CfA echelle database over the years. G.T. acknowledges partial support for this work from NSF grant AST-1007992. The research of M.W. was supported by the Research Program MSM0021620860 "Physical Study of objects and processes in the Solar System and in Astrophysics" of the Ministry of Education of the Czech Republic. We also thank the amateur observers from Ostrava and Valasske Mezirici: K. Hoňková, J. Jurýšek, and L. Šmelcer.

REFERENCES

Agerer, F., & Hubscher, J. 2001, IBVS, 5016
Amores, E. B., & Lepine, J. R. D. 2005, AJ, 130, 659
Baldwin, E. B. 2003, AAVSO: Obs. Min. Timings Ecl. Bin., 8
Baldwin, E. B., & Samolyk, G. 2007, AAVSO: Obs. Min. Timings Ecl. Bin., 12
Biro, I. B., & Borkovits, T. 2000, IBVS, 4967
Borkovits, T., Biro, I. B., Hegedus, T., et al. 2003, IBVS, 5434
Borkovits, T., Biro, I. B., Hegedus, T., et al. 2004, IBVS, 5579
Borkovits, T., Van Cauteron, P., Lampens, P., et al. 2008, IBVS, 5835
Bozkurt, Z. 2011, IBVS, 5978
Brat, L., Šmelcer, L., Kucakova, H., et al. 2008, OEJV, 94
Brat, L., Zejda, M., & Svoboda, P. 2007, OEJV, 74
Cardelli, J. A., Clayton, G. C., & Mathis, S. 1989, ApJ, 345, 245
Casagrande, L., Ramirez, I., Melendez, J., Bessell, M., & Asplund, M. 2010, A&A, 512, 54
Chabrier, G., & Baraffe, I. 2000, ARA&A, 38, 337
Clausen, J. V., Bruntt, H., Claret, A., et al. 2009, A&A, 502, 253
Cutri, R. M., Skrutskie, M. F., van Dyk, S., et al. 2003, The 2MASS All-Sky Catalog of Point Sources (Pasadena, CA: University of Massachusetts and Infrared Processing and Analysis Center (IPAC)/California Institute of Technology)
Diethelm, R. 2005, IBVS, 5653
Diethelm, R. 2006, IBVS, 5713
Diethelm, R. 2007, IBVS, 5781
Diethelm, R. 2009, IBVS, 5894
Diethelm, R. 2010, IBVS, 5920
Diethelm, R. 2011, IBVS, 5960
Diethelm, R. 2012, IBVS, 6029
Dotter, A., Chaboyer, B., Jevremovic, D., et al. 2008, ApJS, 178, 89
Drimmel, R., Cabrera-Lavers, A., & Lopez-Corredoira, M. 2003, A&A, 409, 205
Droege, T. F., Richmond, M. W., & Sallman, M. 2006, PASP, 118, 1666
Eker, Z., Filiz, A. N., Bilir, S., et al. 2008, MNRAS, 389, 1722
Etzel, P. B. 1981, in Photometric and Spectroscopic Binary Systems, ed. C. B. Carling & E. Z. Kopal (Dordrecht: Reidel), 111
Flower, P. J. 1996, ApJ, 469, 355
Grauer, A. D., Neely, A. W., & Lacy, C. H. S. 2008, PASP, 120, 992
Hall, D. S. 1994, MmSAI, 65, 73
Henden, A. A., Levine, S. E., Terrell, D., Smith, T. C., & Welch, D. 2012, JAVSO, 40, 430
Hog, E., Fabricius, C., Makarov, V. V., et al. 2000, A&A, 355, L27
Hubscher, J. 2007, IBVS, 5802
Hubscher, J., Lehmann, P., Monninger, G., Steinbach, H., & Walter, F. 2010, IBVS, 5918
Hubscher, J., Paschke, A., & Walter, F. 2005, IBVS, 5657
Hubscher, J., Steinbach, H., & Walter, F. 2009, IBVS, 5874
Hubscher, J., & Walter, F. 2007, IBVS, 5761
Irwin, J. B. 1952, ApJ, 116, 211
Irwin, J. B. 1959, AJ, 64, 149
Kim, C., Lee, C., Yoon, Y., et al. 2006, IBVS, 5694
Kozyreva, V. S. 1990, Ap&SS, 165, 1
Kozyreva, V. S., Kusakin, A. V., & Khaliullin, Kh. F. 2005, AstL, 31, 117
Lacy, C. H. 1987, AJ, 94, 1035
Lacy, C. H. S. 2002, IBVS, 5357
Lacy, C. H. S. 2003, IBVS, 5487
Lacy, C. H. S. 2004, IBVS, 5577
Lacy, C. H. S. 2006, IBVS, 5670
Lacy, C. H. S. 2007, IBVS, 5764
Lacy, C. H. S. 2009, IBVS, 5910
Lacy, C. H. S. 2011, IBVS, 5972
Lampens, P., Kleidis, S., Van Cauteren, P., et al. 2010, IBVS, 5933
Latham, D. W. 1992, in ASP Conf. Ser. 32, IAU Coll. 135, Complementary Approaches to Double and Multiple Star Research, ed. H. A. McAlister & W. I. Hartkopf (San Francisco, CA: ASP), 110
Latham, D. W., Stefanik, R. P., Torres, G., et al. 2002, AJ, 124, 1144
Liu, X., Cai, Z., & Tan, H. 1989, Ap&SS, 154, 1
Meinunger, L. 1980, Mitt. Verand. Stern (Sonneberg), 8, 121

Nagai, K. 2005, Var. Star Bull. (Japan), 43
Nagai, K. 2006, Var. Star. Bull. (Japan), 44
Nelson, R. H. 2002, IBVS, 5224
Nelson, R. H. 2006, IBVS, 5672
Nelson, R. H. 2010, IBVS, 5929
Nordstrom, B., Latham, D. W., Morse, J. A., et al. 1994, A&A, 287, 338
North, P., & Zahn, J.-P. 2004, NewAR, 48, 741
Paschke, A. 2012, OEJV, 0142
Pizzolato, N., Maggio, A., Micela, G., Sciortini, S., & Ventura, P. 2003, A&A, 397, 147
Popper, D. M. 1980, ARA&A, 18, 115
Popper, D. M. 2000, AJ, 119, 2391
Popper, D. M., & Etzel, P. B. 1981, AJ, 86, 102
Press, W. H., Teukolsky, S. A., Vetterling, W. T., & Flannery, B. P. 1992, Numerical Recipes (2nd ed.; Cambridge: Cambridge Univ. Press), 650
Samolyk, G. 2008, JAVSO, 36, 171
Samolyk, G. 2009, JAVSO, 37, 44
Samolyk, G. 2010, JAVSO, 38, 183
Samolyk, G. 2011, JAVSO, 39, 177
Schlegel, D. J., Finkbeiner, D. P., & Davis, M. 1998, ApJ, 500, 525
Southworth, J., Bruntt, H., & Buzasi, D. L. 2007, A&A, 467, 1215
Strassmeier, K. G., Hall, D. S., Fekel, F. C., & Scheck, M. 1993, A&AS, 100, 173
Strohmeier, B. 1958, Obs, 78, 137
Torres, G. 2010, AJ, 140, 1158
Torres, G., Lacy, C. H., Marschall, L. A., Sheets, H. A., & Mader, J. A. 2006, ApJ, 640, 1018
Torres, G., Neuhauser, R., & Guenther, E. W. 2002, AJ, 123, 1701
Torres, G., Stefanik, R. P., Andersen, J., et al. 1997, AJ, 114, 2764
Torres, G., Vaz, L. P. R., & Lacy, C. H. S. 2008, AJ, 136, 2158
Voges, W., Aschenbach, B., Boller, Th., et al. 1999, A&A, 349, 389
Vos, J., Clausen, J. V., Jorgensen, U. G., et al. 2012, A&A, 540, A64
Wolf, M., & Sarounova, L. 1996, IBVS, 4292
Yi, S., Demarque, P., Kin, Y.-C., et al. 2001, ApJS, 136, 417
Zejda, M., Mikulasek, Z., & Wolf, M. 2006, IBVS, 5741
Zucker, S., & Mazeh, T. 1994, ApJ, 420, 806
Zucker, S., Torres, G., & Mazeh, T. 1995, ApJ, 452, 863